Energy-Efficient Torque-Vectoring Control of Electric Vehicles With Multiple Drivetrains

Giovanni De Filippis, Basilio Lenzo , *Member, IEEE*, Aldo Sorniotti , *Member, IEEE*, Patrick Gruber , and Wouter De Nijs

Abstract—The safety benefits of torque-vectoring control of electric vehicles with multiple drivetrains are well known and extensively discussed in the literature. Also, several authors analyze wheel torque control allocation algorithms for reducing the energy consumption while obtaining the wheel torque demand and reference yaw moment specified by the higher layer of a torque-vectoring controller. Based on a set of novel experimental results, this study demonstrates that further significant energy consumption reductions can be achieved through the appropriate tuning of the reference understeer characteristics. The effects of drivetrain power losses and tire slip power losses are discussed for the case of identical drivetrains at the four vehicle corners. Easily implementable yet effective rule-based algorithms are presented for the set-up of the energy-efficient reference yaw rate, feedforward yaw moment and wheel torque distribution of the torque-vectoring controller.

Index Terms—Drivetrain power loss, tire slip power loss, reference yaw rate, reference yaw moment, wheel torque distribution.

I. INTRODUCTION

A wide literature discusses torque-vectoring (TV) controllers for electric vehicles (EVs) with multiple drivetrains. In particular, the safety and cornering agility benefits of TV have been widely assessed [1]–[11], together with the possibility of generating the reference yaw moment through wheel torque distributions meeting various criteria, including energy efficiency [12]–[32].

G. De Filippis was with the Centre for Automotive Engineering, University of Surrey, Guildford GU2 7XH, U.K. He is now with McLaren Automotive Ltd., Woking GU21 4YH, U.K. (e-mail: giovanni.defilippis@mclaren.com).

B. Lenzo was with the Centre for Automotive Engineering, University of Surrey, Guildford GU2 7XH, U.K. He is now with the Department of Engineering and Mathematics, Sheffield Hallam University, Sheffield S1 1WB, U.K. (e-mail: basilio.lenzo@shu.ac.uk).

A. Sorniotti and P. Gruber are with the Centre for Automotive Engineering, University of Surrey, Guildford GU2 7XH, U.K. (e-mail: a.sorniotti@surrey.ac.uk; p.gruber@surrey.ac.uk).

W. De Nijs is with the Flanders MAKE, Lommel 3920, Belgium (e-mail: wouter.denijs@flandersmake.be).

Color versions of one or more of the figures in this paper are available online at http://ieeexplore.ieee.org.

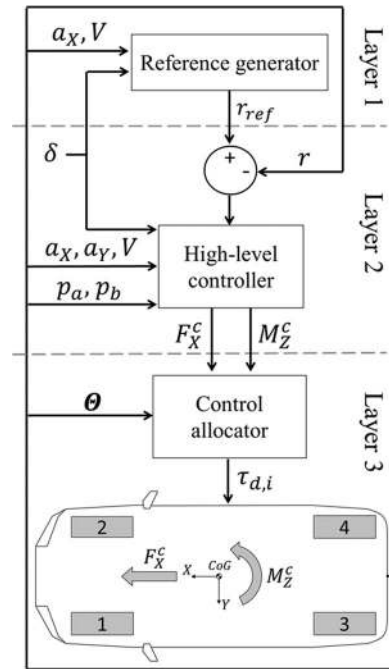Digital Object Identifier 10.1109/TVT.2018.2808186

Fig. 1. Simplified schematic of a typical TV controller for EVs.

Fig. 1 shows the structure of a typical TV controller for an EV with multiple motors. It consists of three layers: i) a reference generator (Layer 1) responsible for defining the target values of the EV outputs (such as the reference yaw rate, r_{ref}) starting from the driver inputs (e.g., the steering wheel angle, δ, and the accelerator and brake pedal positions, p_a and p_b) and the measured or estimated vehicle states (e.g., vehicle speed, V, and longitudinal acceleration, a_X); ii) a high-level controller (Layer 2), generating the overall traction/braking force demand, F_X^c, and yaw moment demand, M_Z^c, to achieve the reference values of the outputs; and iii) a low-level controller (i.e., the 'control allocator', Layer 3), which calculates the reference torques, $\tau_{d,i}$, for the individual wheels, generating the values of F_X^c and M_Z^c.

To the knowledge of the authors, there is a gap in the literature on how to set r_{ref} to minimize the overall power loss for any operating condition of the EV. [27]–[30] are preliminary studies on the topic. However, with the exception of [27], which does not formulate a TV controller, they are not based on experiments at high lateral accelerations. Moreover, [28]–[30] consider only in-wheel drivetrains, and do not account for the significant contribution of the mechanical transmission power losses, typical
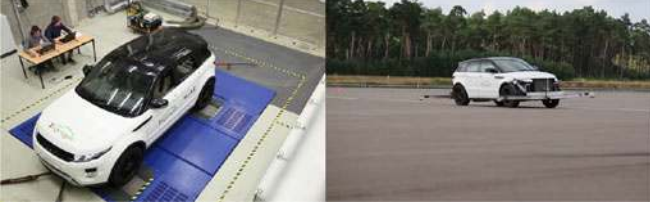
Fig. 2. The Range Rover Evoque EV demonstrator on the rolling road and during a cornering test.
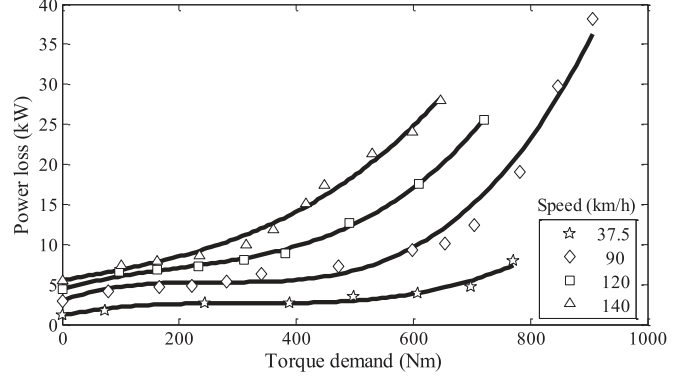

Fig. 3. Experimental points (markers) and cubic polynomial interpolations (continuous lines) of the power loss characteristics of the left front electric drivetrain for different vehicle speeds.

of the more common on-board drivetrains. Finally, the available studies provide useful control design guidelines, but do not reach the stage of developing industrially implementable controllers.

This study addresses the knowledge gap by providing the following contributions:

- The experimental assessment of the influence of the control yaw moment on the energy consumption for a wide range of lateral accelerations.
- The theoretical framework to reveal the influence of the different power loss contributions on the obtained measurements.
- An easily implementable TV controller minimizing the electric drivetrain power losses, and a sub-optimal TV controller including consideration of tire slip power losses as well.
- The preliminary assessment of the proposed strategies through experimental results.

II. EXPERIMENTAL TESTS

Experimental tests were carried out with a fully electric Range Rover Evoque prototype that has four on-board drivetrains (see Fig. 2), each consisting of an inverter, a switched reluctance electric motor, a single-speed transmission, constant velocity joints and a half-shaft.

A. Drivetrain Power Loss Characteristics

The drivetrain power loss characteristics were studied by testing the EV on the MAHA rolling road facility available at Flanders MAKE (Belgium). Fig. 3 reports the measured steady-state power loss characteristics of the left front drivetrain as functions of the respective drivetrain traction torque, $\tau_{d,1,t}$, for multiple vehicle speeds. The subscript '1' indicates the specific drivetrain according to the numbering convention in Fig. 1. The power loss is the difference between the electric input power of the inverter and the mechanical power at the roller. As a consequence, it includes the losses in the inverter, electric motor, mechanical transmission and tire (rolling resistance and longitudinal slip). $\tau_{d,1,t}$ is the net drivetrain torque at the wheel, i.e., $\tau_{d,1,t}$ is calculated as the sum of the wheel torque, measured at the roller, and the rolling resistance torque at that speed.

[26] and [31] show that for a given V the power loss characteristics of the i-th vehicle corner can be approximated through cubic polynomials that are strictly monotonically increasing functions of the generic drivetrain torque, $\tau_{d,i,t/g} \geq 0$, and have

a single inflection point. In formulas:

$$P_{\text{loss},i,t/g}\left(\tau_{d,i,t/g}, \boldsymbol{\Theta}\right) = a_{i,t/g}\left(\boldsymbol{\Theta}\right) \tau_{d,i,t/g}^3$$
$$+ b_{i,t/g}\left(\boldsymbol{\Theta}\right) \tau_{d,i,t/g}^2 + c_{i,t/g}\left(\boldsymbol{\Theta}\right) \tau_{d,i,t/g} + d_i\left(\boldsymbol{\Theta}\right) \quad (1)$$

where the subscripts 't' and 'g' indicate traction and regeneration, respectively, since the drivetrain power loss characteristics can be different in the two cases. The coefficient d_i represents the rolling resistance power loss, which is the same in traction and regeneration. This term includes the contribution of the tire and drivetrain, and is usually expressed as a polynomial function of the angular drivetrain speed, which, in a first approximation, can be considered directly proportional to vehicle speed (through the gear ratio and wheel radius). The resulting formulation is:

$$d_i = F_{Z,i} V \left(f_0 + f_1 V + f_2 V^2\right) + d_{dr,i} \quad (2)$$

where f_0, f_1 and f_2 are the rolling resistance coefficients of the tire, $F_{Z,i}$ is the vertical load on the i-th wheel, and $d_{dr,i}$ is the i-th drivetrain power loss at zero torque, which is an increasing function of speed.

In general, $\boldsymbol{\Theta}$ (see Fig. 1 and (1)) is the vector of relevant parameters, e.g., in addition to vehicle speed it can include the electric motor temperature as well, depending on data availability for the specific drivetrain and the level of sophistication of the analysis. The proposed fitting functions of the power losses in (1): i) are strictly monotonically increasing if $a_{i,t/g} > 0$, $c_{i,t/g} > 0$ and $b_{i,t/g}^2 < 3a_{i,t/g}c_{i,t/g}$; and ii) present an inflection point for $\tau_{d,i,t/g} > 0$ if $b_{i,t/g} < 0$.

Fig. 3 includes the curves resulting from the least-squares fitting of the experimental drivetrain power loss characteristics in traction. At each V a satisfactory agreement is achieved between the fitting curves and the measured points, therefore (1) will be used in the remainder for modeling the power losses.

B. Effect of the Understeer Characteristic

The impact of the reference yaw rate, i.e., the reference understeer characteristic and control yaw moment, on the power consumption was experimentally investigated at the Lommel proving ground (Belgium) on the Evoque EV demonstrator. In
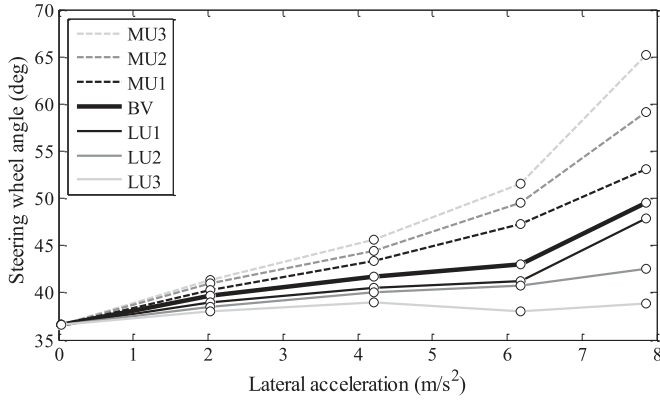
Fig. 4.   Experimentally measured understeer characteristics.

TABLE I
EXPERIMENTAL ENERGY CONSUMPTION ALONG ONE
SKID-PAD LAP ($\sim$60 m RADIUS)

Lateral acceleration (m/s^2)	Optimal yaw moment (Nm)	Energy consumption (Wh)		Improvement of AM wrt BV (%)
		BV	AM	
2	450	75.52	71.44	5.40
4	600	106.48	99.10	6.93
6	850	152.34	141.85	6.89
8	1600	250.24	219.43	12.31

particular, skid-pad tests with a $\sim$60 m radius were performed at constant speeds of $\sim$39, 56, 68 and 79 km/h, corresponding to lateral accelerations, a_Y, of $\sim$2, 4, 6 and 8 m/s^2, with the EV cornering in anti-clockwise direction. The TV controller of [32] was used to track r_{ref}. According to the adopted sign conventions (see Fig. 1), M_Z^c is positive when it is destabilizing the vehicle. A 50:50 front-to-rear torque distribution was used within each side of the EV.

Fig. 4 shows the set of measured understeer characteristics. The EV without TV is indicated as BV (baseline vehicle) and the notations MU and LU in the legend indicate more understeer and less understeer with respect to the BV. Fig. 5 plots the measured power consumptions as functions of M_Z^c for two lateral accelerations (2 m/s^2 and 8 m/s^2), while Table I includes the results for the whole set of a_Y values. The power consumption always presents two minima, i.e., a local minimum (LM) for a stabilizing yaw moment, and an absolute minimum (AM) for a destabilizing yaw moment. At a_Y $\sim$2 m/s^2 (Fig. 5(a)) the difference between the power consumptions corresponding to the LM and AM is very small. However, the difference becomes more significant at greater a_Y, e.g., $\sim$7% at 8 m/s^2 (Fig. 5(b)). Interestingly, the $|M_Z^c|$ value generating the two minima is approximately the same.

In Fig. 5(a) polynomial fitting function is introduced to track the measured power consumption profile. The coefficients of the polynomial are obtained through a weighted least-squares approach that penalizes the most uncertain data, i.e., those with high standard deviations. Based on this procedure, the map of the power consumption isolines is obtained as shown in Fig. 6, where the solid and dashed black lines track the AM and LM
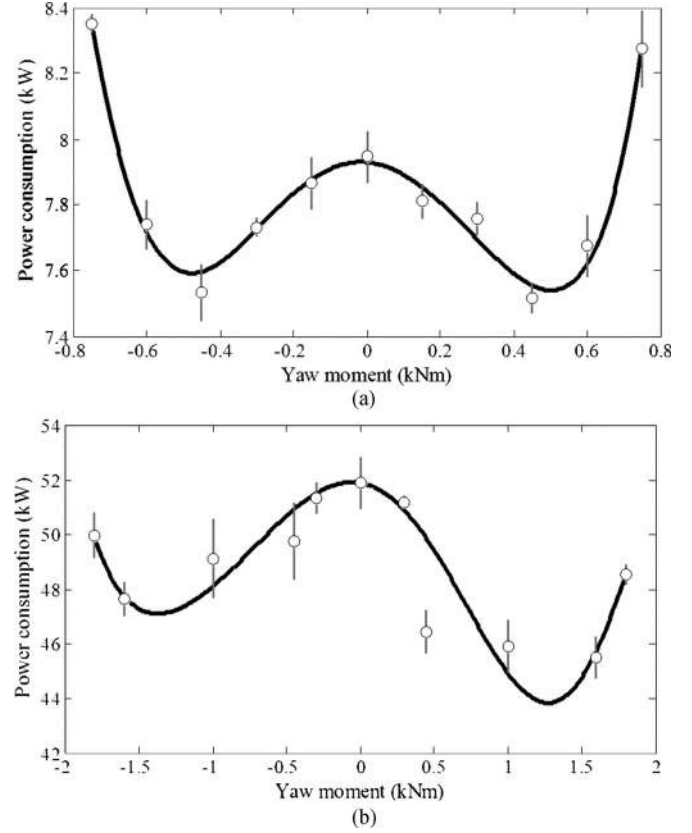

Fig. 5.   Power consumption measured at lateral accelerations of (a) 2 m/s^2 and (b) 8 m/s^2 as a function of M_Z^c. Circles and vertical lines refer to the calculated averages and standard deviations, respectively. The black solid line indicates the polynomial fitting function.
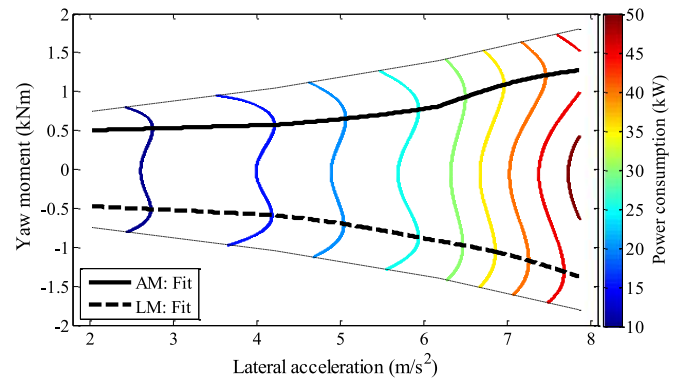
Fig. 6.   Power consumption isolines. AM and LM indicate the fitted global and local minima, respectively. The thin lines indicate the boundaries of the experimentally investigated region.

according to the fitting functions. A less understeering behavior with respect to the BV provokes a significant reduction of the energy consumption (e.g., $\sim$12% at 8 m/s^2, see Table I). The important conclusion is that the cornering behavior of the vehicle, defined in Layer 1 of Fig. 1, influences the energy consumption in cornering at least as much as the control allocator implemented in Layer 3 (for the results of the latter on the same EV refer to [26] and [31]).

Fig. 7. $\tau_{d,\mathrm{switch},t}$ as a function of V for the case study EV.
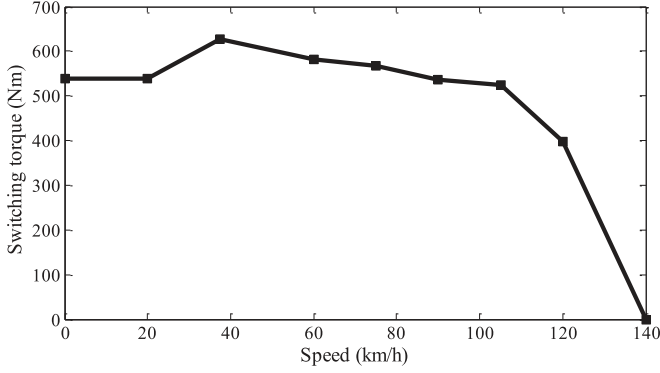
III. PROBLEM FORMULATION

A. Hypotheses and Results From Previous Studies

[26] demonstrates that the energy consumption on a side (left or right) of an EV with four motors is reduced if both drivetrains work either in traction or regeneration, or if one drivetrain is switched off, with respect to the condition of one drivetrain in traction and the other one in regeneration. This is under the assumption that the power loss characteristic of the i-th drivetrain, $P_{\mathrm{loss},i,t/g}$ $(\tau_{d,i,t/g}, \; \boldsymbol{\Theta})$, is positive and strictly monotonically increasing as a function of the drivetrain torque, i.e., $P_{\mathrm{loss},i,t/g}(\tau_{d,i,t/g}, \; \boldsymbol{\Theta}) > 0$ and $\partial P_{\mathrm{loss},i,t/g}(\tau_{d,i,t/g}, \boldsymbol{\Theta})/\partial \tau_{d,i,t/g} > 0$.

Under the additional hypothesis of equal drivetrains on the front and rear axles, and by neglecting the effect of tire slip, [26] proves that the most efficient control allocation strategy on an individual side is based on the switching from a single wheel strategy (SWS) to an even distribution strategy (EDS) when the absolute value of the torque demand on side reaches the threshold $\tau_{d,\mathrm{switch},t/g}(\boldsymbol{\Theta}) \geq 0$ given by:

$$P_{\mathrm{loss},t/g}\left(\tau_{d,\mathrm{switch},t/g}, \boldsymbol{\theta}\right) + P_{\mathrm{loss},t/g}\left(0, \boldsymbol{\theta}\right)$$
$$= 2 P_{\mathrm{loss},t/g}\left(\tau_{d,\mathrm{switch},t/g}/2, \boldsymbol{\theta}\right) \qquad (3)$$

By combining (1) and (3), the threshold is given by $\tau_{d,\mathrm{switch},t/g} = -2b_{1,t/g}/(3a_{1,t/g}) \geq 0$. Fig. 7 plots $\tau_{d,\mathrm{switch},t}$ as a function of V by using the experimental data in Fig. 3. In the specific case $\tau_{d,\mathrm{switch},t}$ is zero at 140 km/h because of the convex shape of the respective power loss characteristic.

B. Properties of the Power Loss Characteristic on an EV Side

The torque demands on the individual drivetrains, $\tau_{d,i} \gtrless 0$, can be expressed as functions of the total torque demands on that side, $\tau_{d,l} \gtrless 0$ and $\tau_{d,r} \gtrless 0$, and the torque shifts with respect to the even distribution on that side, $\varepsilon_{d,l}(\tau_{d,l}, \boldsymbol{\Theta})$ and $\varepsilon_{d,r}(\tau_{d,r}, \boldsymbol{\Theta})$:

$$\tau_{d,1} = \frac{\tau_{d,l}}{2} + \varepsilon_{d,l}; \; \tau_{d,3} = \frac{\tau_{d,l}}{2} - \varepsilon_{d,l};$$
$$\tau_{d,2} = \frac{\tau_{d,r}}{2} + \varepsilon_{d,r}; \; \tau_{d,4} = \frac{\tau_{d,r}}{2} - \varepsilon_{d,r} \qquad (4)$$

The subscripts 'l' and 'r' indicate the left- and right-hand sides of the EV. $\tau_{d,l}$ and $\tau_{d,r}$ are obtained from the longitudinal force and yaw moment balance equations (without considering rolling resistance):

$$\tau_{d,l} = \left(F_X^c - \frac{M_Z^c}{w}\right)\frac{R}{2}; \; \tau_{d,r} = \left(F_X^c + \frac{M_Z^c}{w}\right)\frac{R}{2} \qquad (5)$$

where w is the half-track width and R is the wheel radius.

The power losses on each side in traction or regeneration, $P_{\mathrm{loss},l,t/g}$ and $P_{\mathrm{loss},r,t/g}$, are:

$$P_{\mathrm{loss},l,t/g}\left(\tau_{d,l}, \varepsilon_{d,l}, \boldsymbol{\Theta}\right) = P_{\mathrm{loss},1,t/g}\left(\left|\frac{\tau_{d,l}}{2} + \varepsilon_{d,l}\right|\right)$$
$$+ P_{\mathrm{loss},3,t/g}\left(\left|\frac{\tau_{d,l}}{2} - \varepsilon_{d,l}\right|\right)$$

$$P_{\mathrm{loss},r,t/g}\left(\tau_{d,r}, \varepsilon_{d,r}, \boldsymbol{\Theta}\right) = P_{\mathrm{loss},2,t/g}\left(\frac{\tau_{d,r}}{2} + \varepsilon_{d,r}\right)$$
$$+ P_{\mathrm{loss},4,t/g}\left(\left|\frac{\tau_{d,r}}{2} - \varepsilon_{d,r}\right|\right) \qquad (6)$$

Under appropriate conditions the overall power loss on a side is a strictly monotonically increasing function of the absolute value of the torque demand on that side. By referring to the left-hand side it is:

$$\frac{\partial P_{\mathrm{loss},l,t/g}}{\partial |\tau_{d,l}|} = \frac{\partial P_{\mathrm{loss},1,t/g}}{\partial |\tau_{d,1}|}\frac{\partial |\tau_{d,1}|}{\partial |\tau_{d,l}|} + \frac{\partial P_{\mathrm{loss},3,t/g}}{\partial |\tau_{d,3}|}\frac{\partial |\tau_{d,3}|}{\partial |\tau_{d,l}|}$$
$$= A + \frac{\partial |\varepsilon_{d,l}|}{\partial |\tau_{d,l}|} B$$
$$A = \frac{1}{2}\left(\frac{\partial P_{\mathrm{loss},1,t/g}}{\partial |\tau_{d,1}|} + \frac{\partial P_{\mathrm{loss},3,t/g}}{\partial |\tau_{d,3}|}\right)$$
$$B = \frac{\partial P_{\mathrm{loss},1,t/g}}{\partial |\tau_{d,1}|} - \frac{\partial P_{\mathrm{loss},3,t/g}}{\partial |\tau_{d,3}|} \qquad (7)$$

Based on Section III-A, the optimal torque distribution strategy for the case of identical drivetrains is:

$$\begin{cases} \varepsilon_{d,l,t/g}^*\left(\tau_{d,l}, \boldsymbol{\Theta}\right) = \pm\dfrac{\tau_{d,l}}{2} & \text{if } |\tau_{d,l}| < \tau_{d,\mathrm{switch},t/g} \\[2mm] \varepsilon_{d,l,t/g}^*\left(\tau_{d,l}, \boldsymbol{\Theta}\right) = 0 & \text{if } |\tau_{d,l}| \geq \tau_{d,\mathrm{switch},t/g} \end{cases} \qquad (8)$$

where the superscript '$*$' indicates the optimality of the solution. By combining (7) and (8) it can be demonstrated that $\partial P_{\mathrm{loss},l,t/g}/\partial|\tau_{d,l}| > 0$ is always met with identical drivetrains (see Appendix A). In summary, it is:

$$\frac{\partial P_{\mathrm{loss},l,t/g}}{\partial |\tau_{d,l}|} > 0 \Leftrightarrow \begin{cases} \dfrac{\partial |\varepsilon_{d,l}|}{\partial |\tau_{d,l}|} > -\dfrac{A}{B} \text{ if } B > 0 \\[2mm] \dfrac{\partial |\varepsilon_{d,l}|}{\partial |\tau_{d,l}|} < -\dfrac{A}{B} \text{ if } B < 0 \\[2mm] \text{always in case of equal drivetrains} \end{cases} \qquad (9)$$

C. Optimal Traction-Regeneration Balance

Based on the hypotheses of Sections III-A and III-B, this section proves that the total drivetrain power loss for a generic

operating condition of the EV – including cornering – is minimized when all active drivetrains operate either in traction or regeneration.

Let us consider an EV with $\partial P_{\mathrm{loss},l,t/g}/\partial |\tau_{d,l}| > 0$ and $\partial P_{\mathrm{loss},r,t/g}/\partial |\tau_{d,r}| > 0$. If $\tau_{d,\mathrm{tot}} = F_X^c R \geq 0$ and only one side is active, for example $\tau_{d,l,or} = \tau_{d,\mathrm{tot}}$ and $\tau_{d,r,or} = 0$ (the subscript 'or' stands for original distribution), the control yaw moment is $M_{Z,or}^c = -\tau_{d,\mathrm{tot}} w/R$. If $M_{Z,\mathrm{new}}^c < M_{Z,or}^c$ is considered for the same $\tau_{d,\mathrm{tot}}$, a regenerative torque $\bar{\tau}_d > 0$ must be applied on the right-hand side, thus bringing $\tau_{d,r,\mathrm{new}} = -\bar{\tau}_d$ and $\tau_{d,l,\mathrm{new}} = \tau_{d,l,or} + \bar{\tau}_d$. The extra amount of power drawn by the left drivetrains is $\bar{\tau}_d(V/R) + \Delta P_{\mathrm{loss},l,t}$, with respect to the initial case of $\tau_{d,l,or} = \tau_{d,\mathrm{tot}}$. The extra power regenerated by the right drivetrains is $\bar{\tau}_d(V/R) - \Delta P_{\mathrm{loss},r,g}$, with respect to the initial case of $\tau_{d,r,or} = 0$. Their difference is positive, i.e., the overall power loss increases. In fact, since $P_{\mathrm{loss},l,t}$ and $P_{\mathrm{loss},r,g}$ are positive and strictly monotonically increasing functions of $|\tau_{d,l}|$ and $|\tau_{d,r}|$, it is:

$$
\begin{aligned}
\Delta P_{\mathrm{loss},t} &= P_{\mathrm{loss},l,t}\left(\tau_{d,l,or} + \bar{\tau}_d, \varepsilon_{d,l}^*\left(\tau_{d,\mathrm{tot}} + \bar{\tau}_d, \boldsymbol{\Theta}\right), \boldsymbol{\Theta}\right) \\
&\quad - P_{\mathrm{loss},l,t}\left(\tau_{d,\mathrm{tot}}, \varepsilon_{d,l}^*\left(\tau_{d,\mathrm{tot}}, \boldsymbol{\Theta}\right), \boldsymbol{\Theta}\right) > 0 \\
\Delta P_{\mathrm{loss},g} &= P_{\mathrm{loss},r,g}\left(\bar{\tau}_d, \varepsilon_{d,r}^*\left(\bar{\tau}_d, \boldsymbol{\Theta}\right), \boldsymbol{\Theta}\right) \\
&\quad - P_{\mathrm{loss},r,g}\left(0, \varepsilon_{d,r}^*\left(0, \boldsymbol{\Theta}\right), \boldsymbol{\Theta}\right) > 0
\end{aligned}
\tag{10}
$$

Similarly, for $\tau_{d,\mathrm{tot}} < 0$, the introduction of any traction torque demand on the left-hand side increases the overall power loss.

In conclusion, in case of equal drivetrains on the front and rear axles, both the right- and left-hand sides (if active) must work either in traction or regeneration. By combining this condition with the one in Section III-A referred to each individual side, all the active drivetrains must simultaneously operate in traction or regeneration, to minimize the total drivetrain power loss. As a consequence, during TV M_Z^c has to be limited between thresholds. In fact, if $F_X^c \geq 0$ (traction), each EV side has to be in traction (or switched off), i.e., $\tau_{d,l}, \tau_{d,r} \geq 0$. If $F_X^c < 0$ (braking), each EV side has to be in regeneration (or switched off), i.e., $\tau_{d,l}, \tau_{d,r} \leq 0$. By imposing these conditions, the boundaries of the optimal yaw moment demand, M_Z^{c*}, are:

$$
-|F_X^c|\, w \leq M_Z^{c*} \leq |F_X^c|\, w
\tag{11}
$$

D. Cost Function Formulation

The cost function $J(\boldsymbol{\tau}_D, \boldsymbol{\Theta})$, equal to the sum of the four drivetrain power losses, is used to find the optimal value of M_Z^c. $\boldsymbol{\tau}_D$ is the vector of the four drivetrain torques. For the sake of conciseness the following formulations will be presented for an EV in traction ($F_X^c \geq 0$), and the subscript 't' will be omitted as the calculations can be carried out independently for traction and regeneration (see Sections III-A–III-C).
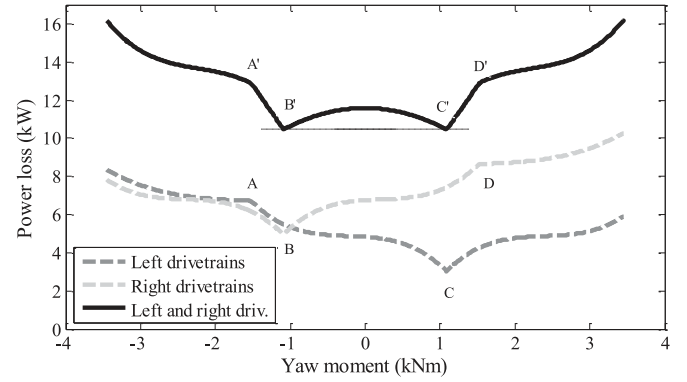

Fig. 8. Drivetrain power loss contributions as functions of M_Z^c at $V = 60$ km/h, $a_X = 0.5$ m/s^2 and $a_Y = 4$ m/s^2.

By considering equal motor speeds at the four EV corners, and using (1) and (4) in traction, $J(\boldsymbol{\tau}_D, \boldsymbol{\Theta})$ is:

$$
\begin{aligned}
J\left(\boldsymbol{\tau}_D, \boldsymbol{\Theta}\right) &= \frac{a_1}{4}\left(\tau_{d,l}^3 + \tau_{d,r}^3\right) + \frac{b_1}{2}\left(\tau_{d,l}^2 + \tau_{d,r}^2\right) \\
&\quad + 3a_1\left(\varepsilon_{d,l}^2 \tau_{d,l} + \varepsilon_{d,r}^2 \tau_{d,r}\right) + c_1\left(\tau_{d,l} + \tau_{d,r}\right) \\
&\quad + 2b_1\left(\varepsilon_{d,l}^2 + \varepsilon_{d,r}^2\right) + \sum_{i=1}^{4} d_i \\
&\qquad \text{for } \tau_{d,l}, \tau_{d,r} > 0
\end{aligned}
\tag{12}
$$

Based on (5), $\tau_{d,l}$ and $\tau_{d,r}$ in (12) can be expressed as functions of F_X^c and M_Z^c. In a first approximation, if the lateral tire slip power losses are neglected, the overall traction/braking force demand, F_X^c, can be calculated as:

$$
F_X^c = m_{eq} a_X + F_{X,dr} + F_{X,sl} + \sum_{i=1}^{4} \frac{\tau_{rr,i}}{R}
\tag{13}
$$

where m_{eq} is the apparent mass of the EV, $F_{X,dr}$ and $F_{X,sl}$ are the aerodynamic drag force and road grade force, and $\tau_{rr,i}$ is the rolling resistance torque at the $i-$th wheel [33].

For example, by combining (4), (8), (12) and (13), Fig. 8 reports the left and right drivetrain power losses and their sum, i.e., J, as functions of M_Z^c, for the case of equal drivetrain power loss characteristics in traction and regeneration. When the EV is negotiating a left-hand turn ($a_Y > 0$), the right side exhibits a larger power loss due to the increase of tire rolling resistance induced by the vertical load transfer. The vertical tire loads were calculated using the load transfer equations for steady-state conditions (see [33] and [34]).

In particular, in Fig. 8, point A corresponds to the activation of the second drivetrain on the left-hand vehicle side at $\tau_{d,\mathrm{switch}}$, i.e., on the left of A, both left drivetrains are operating in traction. D corresponds to the same situation as A for the right drivetrains. On the left of C it is $\tau_{d,l} > 0$, and it is $\tau_{d,l} < 0$ on the right of C. At C, the left drivetrains are switched off. B is the equivalent of C for the right drivetrains. As a consequence, in the graph of J the points on the left of A' and on the right of D' imply the simultaneous operation of three drivetrains, with

$\tau_{d,l}\tau_{d,r} < 0$. Between A' and D' two drivetrains are active, i.e., one per side. In particular, between B' and C' both sides are in traction. Between A' and B' and between C' and D' one side is in traction and the other one is in regeneration, and the consumption increases with respect to the zone between B' and C' as demonstrated in Section III-C. Interestingly, the shape of J in Fig. 8 is rather similar to the one of the experimentally measured power consumption of Fig. 5, despite the total drivetrain power loss in Fig. 8 is symmetric with two minima corresponding to B' and C', while the experimental power consumption is not. B' and C' correspond to the yaw moment limits defined in (11).

Based on the simplified model used for Fig. 8, the sum of the rolling resistance power losses does not vary with M_Z^c. As a consequence, the rolling resistance contribution can be eliminated from J in (12), leading to the following cost function $\bar{J}$:

$$\bar{J}(\tau_{d,l}, \tau_{d,r}, \varepsilon_{d,l}, \varepsilon_{d,r}, \boldsymbol{\Theta}) = J - \sum_{i=1}^{4} d_i \qquad (14)$$

Through (5) $\bar{J}(\tau_{d,l}, \tau_{d,r}, \varepsilon_{d,l}, \varepsilon_{d,r}, \boldsymbol{\Theta})$ can be reformulated as $\bar{J}(M_Z^c, F_X^c, \varepsilon_{d,l}, \varepsilon_{d,r}, \boldsymbol{\Theta})$. This will be used in Section IV for deriving the analytical expressions of M_Z^c minimizing the total drivetrain power loss. For ease of notation, $\boldsymbol{\Theta}$ will be omitted in the remainder of the paper.

IV. YAW MOMENT MINIMIZING THE DRIVETRAIN POWER LOSSES

This section, firstly, investigates how the shape of $\bar{J}$ as a function of M_Z^c changes with F_X^c; and, secondly, calculates the optimal value of M_Z^c, indicated as M_Z^{c*}.

A. Analytical Derivation

The minimization of the drivetrain power losses is achieved with the activation of a different number of drivetrains, depending on F_X^c. From the discussions in Sections III-A–III-D, the M_Z^c values corresponding to the switching from SWS to EDS within the EV sides are:

$$\tau_{d,r} = \tau_{d,\text{switch}} \Leftrightarrow M_Z^c = \bar{M}_Z^c = \left(\frac{2\tau_{d,\text{switch}}}{R} - F_X^c\right) w$$

$$\tau_{d,l} = \tau_{d,\text{switch}} \Leftrightarrow M_Z^c = -\bar{M}_Z^c = \left(F_X^c - \frac{2\tau_{d,\text{switch}}}{R}\right) w \qquad (15)$$

Based on (15) and the analysis of $\bar{J}$, the following Cases 1–7 are identified, each of them corresponding to a range of F_X^c.

Case 1: This case is defined by the inequality:

$$\bar{M}_Z^c > F_X^c w \rightarrow 0 < F_X^c < \frac{\tau_{d,\text{switch}}}{R} \qquad (16)$$

In Case 1 both EV sides operate with SWS, thus the cost function in (14) is renamed as $\bar{J}_{Case\,1} = \bar{J}_{\text{SWS+SWS}}$, where the subscript '$SWS + SWS$' indicates the single wheel strategy

on the left and right drivetrains. In formulas:

$$\bar{J}_{\text{Case1}} = \bar{J}_{\text{SWS+SWS}} = \bar{J}\left(M_Z^c, F_X^c, \varepsilon_{d,l} = \frac{\tau_{d,l}}{2}, \varepsilon_{d,r} = \frac{\tau_{d,r}}{2}\right)$$

$$= \frac{3a_1 F_X^c R^3 + 2b_1 R^2}{4w^2} M_Z^{c2}$$

$$+ \frac{a_1 F_X^{c3} R^3 + 2b_1 F_X^{c2} R^2 + 4c_1 F_X^c R}{4} \qquad (17)$$

The analysis of the first and second derivatives of $\bar{J}_{\text{SWS+SWS}}$ shows:

$$\frac{\partial \bar{J}_{\text{SWS+SWS}}}{\partial M_Z^c} = 0 \Leftrightarrow M_Z^c = 0$$

$$\left.\frac{\partial^2 \bar{J}_{\text{SWS+SWS}}}{\partial M_Z^{c\,2}}\right|_0 > 0 \Leftrightarrow F_X^c > \frac{\tau_{d,\text{switch}}}{R} \rightarrow \text{not satisfied} \qquad (18)$$

This means that in Case 1 there are two global minima located at the boundaries of the M_Z^c interval in (11), i.e., $M_Z^{c*} = \pm F_X^c w$. In fact, the normalized cost function $\bar{J}_{\text{Case 1}}/\max(\bar{J}_{\text{Case 1}})$ presents the shape of a non-convex parabola (Fig. 9(1)), which is the same situation as in Fig. 8.

Case 2: In this case $F_X^c = \tau_{d,\text{switch}}/R$. Case 2 is the boundary between Case 1 and Case 3. The value of the cost function $\bar{J}_{\text{Case 2}}$ does not vary with M_Z^c (see Fig. 9(2)), thus any $-F_X^c w \leq M_Z^c \leq F_X^c w$ is optimal.

Case 3: This case is valid for:

$$\frac{\tau_{d,\text{switch}}}{R} < F_X^c < \frac{9\tau_{d,\text{switch}}}{5R} \qquad (19)$$

In this interval $\bar{J} = \bar{J}_{\text{Case 3}}$ turns into a piecewise function:

$$\bar{J}_{\text{Case 3}} = \begin{cases} \bar{J}_{\text{SWS+SWS}} & \text{for } -\bar{M}_Z^c < M_Z^c < \bar{M}_Z^c \\ \bar{J}_{\text{SWS+EDS}} & \text{for } \bar{M}_Z^c < M_Z^c < F_X^c w \\ \bar{J}_{\text{EDS+SWS}} & \text{for } -F_X^c w < M_Z^c < -\bar{M}_Z^c \end{cases} \qquad (20)$$

where the superscripts '$SWS + EDS$' and '$EDS + SWS$' indicate that one vehicle side operates with SWS while the other side operates with EDS, according to the energy efficient wheel torque distribution criterion discussed in Section III-A. In formulas:

$$\bar{J}_{\text{SWS+EDS}}(M_Z^c, F_X^c) = \bar{J}\left(M_Z^c, F_X^c, \varepsilon_{d,l} = \frac{\tau_{d,l}}{2}, \varepsilon_{d,r} = 0\right)$$

$$= -\frac{3R^3 a_1}{32w^3} M_Z^{c3} + \frac{15 F_X^c a_1 R^3 + 12 b_1 R^2}{32w^2} M_Z^{c2}$$

$$- \frac{9a_1 F_X^{c2} R^3 + 8b_1 F_X^c R^2}{32w} M_Z^c$$

$$+ \frac{5a_1 F_X^{c3} R^3 + 12 b_1 F_X^{c2} R^2 + 32 c_1 F_X^c R}{32}$$

$$\bar{J}_{\text{EDS+SWS}}(M_Z^c, F_X^c) = \bar{J}_{\text{SWS+EDS}}(-M_Z^c, F_X^c) \qquad (21)$$
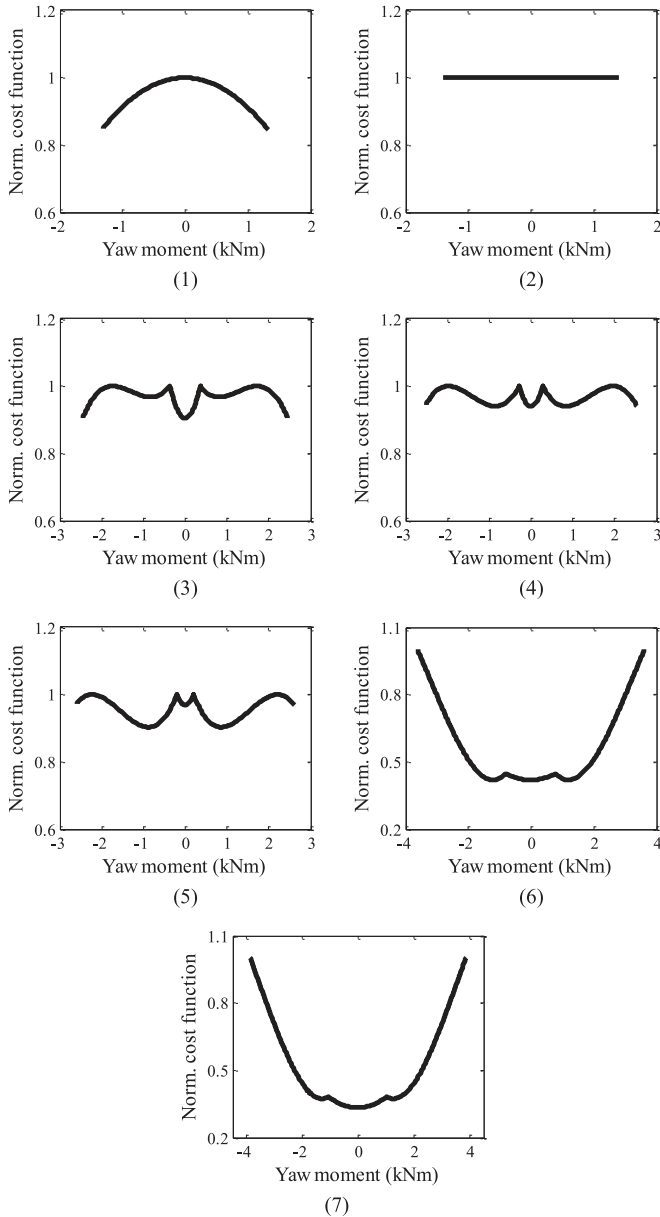
Fig. 9.   Normalized cost function ($\bar{J}/\max(\bar{J})$) as a function of M_Z^c at $V = 37.5$ km/h for the different cases in Section IV (note that these results are independent of a_X and a_Y).

From (18) it follows that the minimum of $\bar{J}_{\mathrm{SWS+SWS}}$ is located at $M_Z^c = 0$, where:

$$\bar{J}_{\mathrm{SWS+SWS}}\left(M_Z^c = 0, F_X^c\right) = \frac{F_X^{c3} R^3 a_1 + 2 F_X^{c2} R^2 b_1 + 4 F_X^c R c_1}{4} \tag{22}$$

The minima of $\bar{J}_{\mathrm{SWS+EDS}}$ and $\bar{J}_{\mathrm{EDS+SWS}}$ are found by imposing:

$$\frac{\partial \bar{J}_{\mathrm{SWS+EDS}}}{\partial M_Z^c} = A_{\bar{J}_{\mathrm{SWS+ESD}}} M_Z^{c2} + B_{\bar{J}_{\mathrm{SWS+EDS}}} M_Z^c$$

$$+ C_{\bar{J}_{\mathrm{SWS+EDS}}} = 0$$

$$A_{\bar{J}_{\mathrm{SWS+EDS}}} = -\frac{9R^3 a_1}{32 w^3}; B_{\bar{J}_{\mathrm{SWS+EDS}}} = \frac{15 F_X^c a_1 R^3 + 12 b_1 R^2}{16 w^2}$$

$$C_{\bar{J}_{\mathrm{SWS+EDS}}} = -\frac{9 a_1 F_X^{c2} R^3 + 8 b_1 F_X^c R^2}{32 w} \tag{23}$$

Since the discriminant Δ of the solution of the second order equation in (23) is always positive, the solutions $M_{Z,1/2}^c$ of (23) are real-valued:

$$\Delta > 0 \Leftrightarrow (b_1 + a_1 F_X^c R)^2 > 0 \rightarrow \text{satisfied} \tag{24}$$

Thus, it is:

$$M_{Z,1/2}^c = \frac{\left(4 b_1 + 5 F_X^c R a_1 \pm 4 |b_1 + F_X^c R a_1|\right) w}{3 R a_1} \tag{25}$$

The contribution $\bar{J}_{\mathrm{EDS+SWS}}$ in (20) is minimized or maximized at $M_Z^c = -M_{Z,1/2}^c$. The term $|b_1 + F_X^c R a_1|$ yields two sub-cases, i.e., Case 3(a) and Case 3(b).

Case 3(a) is valid for:

$$b_1 + F_X^c R a_1 < 0 \rightarrow \frac{\tau_{d,\mathrm{switch}}}{R} < F_X^c < \frac{3}{2} \frac{\tau_{d,\mathrm{switch}}}{R} \tag{26}$$

In this interval, $M_{Z,1}^c$ in (25) becomes:

$$M_{Z,1}^c = \left(3 F_X^c - \frac{4 \tau_{d,\mathrm{switch}}}{R}\right) w \tag{27}$$

It must be verified whether $M_{Z,1}^c$ satisfies the condition in (20) for the existence of $\bar{J}_{\mathrm{SWS+EDS}}$, i.e., $\bar{M}_Z^c < M_{Z,1}^c < F_X^c w$:

$$M_{Z,1}^c < F_X^c w \Leftrightarrow F_X^c < \frac{2 \tau_{d,\mathrm{switch}}}{R} \rightarrow \text{satisfied}$$

$$M_{Z,1}^c > \bar{M}_Z^c \Leftrightarrow F_X^c > \frac{3}{2} \frac{\tau_{d,\mathrm{switch}}}{R} \rightarrow \text{not satisfied} \tag{28}$$

This means that $M_{Z,1}^c$ is outside the relevant M_Z^c interval and must be discarded. The other optimal solution in (25), $M_{Z,2}^c$, is:

$$M_{Z,2}^c = \frac{F_X^c w}{3} \tag{29}$$

$M_{Z,2}^c$ has to be discarded as well, because (together with (26)) it does not satisfy the conditions in (20).

Two additional minima are present at the interval boundaries of $\bar{J}_{\mathrm{SWS+EDS}}$ and $\bar{J}_{\mathrm{EDS+SWS}}$. In fact, it is:

$$\bar{J}_{\mathrm{SWS+EDS}}\left(M_Z^c = F_X^c w, F_X^c\right) = \bar{J}_{\mathrm{EDS+SWS}}(M_Z^c$$

$$= -F_X^c w, F_X^c) = \bar{J}_{\mathrm{SWS+SWS}}\left(M_Z^c = 0, F_X^c\right) \tag{30}$$

In conclusion, in Case 3(a) there are three global minima, located at $M_Z^{c*} = 0$ and $M_Z^{c*} = \pm F_X^c w$.

Case 3(b) is valid for:

$$b_1 + F_X^c R a_1 > 0 \rightarrow \frac{3}{2} \frac{\tau_{d,\mathrm{switch}}}{R} < F_X^c < \frac{9}{5} \frac{\tau_{d,\mathrm{switch}}}{R} \tag{31}$$

In this case $M_{Z,1}^c$ and $M_{Z,2}^c$ lie in the interval of existence of $\bar{J}_{\text{SWS+EDS}}$ (see (20)). Moreover it is:

$$\left.\frac{\partial^2 \bar{J}_{\text{SWS+EDS}}}{\partial M_Z^{c2}}\right|_{M_{Z,1}^c} = -\frac{3R^2 \left(b_1 + F_X^c R a_1\right)}{4w^2} < 0$$

because $b_1 + F_X^c R a_1 > 0$

$$\left.\frac{\partial^2 \bar{J}_{\text{SWS+EDS}}}{\partial M_Z^{c2}}\right|_{M_{Z,2}^c} = \frac{3R^2 \left(b_1 + F_X^c R a_1\right)}{4w^2} > 0$$

because $b_1 + F_X^c R a_1 > 0$ (32)

The same process is applicable to $\bar{J}_{\text{EDS+SWS}}$. This means that there are two local maxima located at $\pm M_{Z,1}^c$ and two local minima located at $\pm M_{Z,2}^c$. By comparing the two minima in $\pm M_{Z,2}^c$ with the minima discussed for Case 3(a), which are still present in this interval, it is:

$$\begin{aligned}
\bar{J}_{\text{SWS+SWS}} \left(0, F_X^c\right) &= \bar{J}_{\text{SWS+EDS}} \left(F_X^c w, F_X^c\right) \\
&= \bar{J}_{\text{EDS+SWS}} \left(-F_X^c w, F_X^c\right) \\
&< \bar{J}_{\text{SWS+EDS}} \left(M_{Z,2}^c, F_X^c\right) \\
&= \bar{J}_{\text{EDS+SWS}} \left(-M_{Z,2}^c, F_X^c\right) \\
&\Leftrightarrow F_X^c < \frac{9}{5}\frac{\tau_{d,SW}}{R}
\end{aligned}$$ (33)

The expression in (33) is obtained through the steps from (45) to (47) in Appendix B.

In summary, as shown in Fig. 9(3), in Case 3(b), i.e., for $3\tau_{d,\text{switch}}/(2R) < F_X^c < 9\tau_{d,\text{switch}}/(5R)$ there are three global minima located at $M_Z^{c*} = 0$ and $M_Z^{c*} = \pm F_X^c w$ (they are the same as for Case 3(a)); two local minima located at $\pm M_{Z,2}^c$; and two local maxima located at $\pm M_{Z,1}^c$.

Case 4: This case is defined for $F_X^c = 9\tau_{d,\text{switch}}/(5R)$. In Case 4 the five minima of Case 3(b) become global minima, as they correspond to the same value of the electric drivetrain power loss. Hence, the optimal values of the reference yaw moment are $M_Z^{c*} = 0$, $M_Z^{c*} = \pm F_X^c w$ and $M_Z^{c*} = \pm F_X^c w/3$. The shape of the cost function is shown in Fig. 9(4).

Case 5: This case is valid for:

$$\frac{9}{5}\frac{\tau_{d,\text{switch}}}{R} < F_X^c < \frac{18}{7}\frac{\tau_{d,\text{switch}}}{R}$$ (34)

Case 5 can be discussed through two sub-cases, 5(a) and 5(b). Case 5(a) is defined for $9\tau_{d,\text{switch}}/(5R) < F_X^c \leq 2\tau_{d,\text{switch}}/R$. Case 5(a) is similar to Case 3 (see (33)). However, the two minima located at $\pm M_{Z,2}^c$ become the only two global minima for the relevant range of F_X^c (Fig. 9 (5)).

The lower boundary of F_X^c for Case 5(b) is defined by:

$$-F_X^c w < \bar{M}_Z^c < 0 \rightarrow F_X^c > \frac{2\tau_{d,\text{switch}}}{R}$$ (35)

In this interval, $\bar{J} = \bar{J}_{\text{Case 5(b)}}$ turns into a piecewise expression:

$$\bar{J}_{\text{Case 5(b)}} = \begin{cases} \bar{J}_{\text{EDS+EDS}} & \text{for } -\bar{M}_Z^c < M_Z^c < \bar{M}_Z^c \\ \bar{J}_{\text{SWS+EDS}} & \text{for } \bar{M}_Z^c < M_Z^c < F_X^c w \\ \bar{J}_{\text{EDS+SWS}} & \text{for } -F_X^c w < M_Z^c < -\bar{M}_Z^c \end{cases}$$ (36)

where:

$$\begin{aligned}
\bar{J}_{\text{EDS+EDS}} \left(M_Z^c, F_X^c\right) &= \frac{3a_1 F_X^c R^3 + 2b_1 R^2}{16w^2} M_Z^{c2} \\
&+ \frac{a_1 F_X^{c3} R^3 + 4b_1 F_X^{c2} R^2 + 16c_1 F_X^c R}{16}
\end{aligned}$$ (37)

The minimum of $\bar{J}_{\text{EDS+EDS}}$ is calculated from:

$$\frac{\partial \bar{J}_{\text{EDS+EDS}}}{\partial M_Z^c} = 0 \Leftrightarrow M_Z^c = 0$$

$$\left.\frac{\partial^2 \bar{J}_{\text{EDS+EDS}}}{\partial M_Z^{c2}}\right|_0 > 0 \Leftrightarrow F_X^c > \frac{\tau_{d,\text{switch}}}{R} \rightarrow \text{satisfied}$$ (38)

which means that there is a local minimum at $M_Z^c = 0$. In this interval, for $\bar{J}_{\text{SWS+EDS}}$ and $\bar{J}_{\text{EDS+SWS}}$ only the condition of existence of $M_{Z,2}^c$ is satisfied, which implies other two local minima at $\pm M_{Z,2}^c$. The values of the cost functions for the three minima are now compared:

$$\begin{aligned}
\bar{J}_{\text{SWS+EDS}} \left(M_{Z,2}^c, F_X^c\right) &= \bar{J}_{\text{SWS+EDS}} \left(-M_{Z,2}^c, F_X^c\right) \\
&< \bar{J}_{\text{EDS+EDS}} \left(M_Z^c = 0, F_X^c\right) \\
&\Leftrightarrow F_X^c < \frac{18}{7}\frac{\tau_{d,\text{switch}}}{R} \rightarrow \text{satisfied}
\end{aligned}$$ (39)

The expression in (39) is obtained through (48)-(49) in Appendix B. $F_X^c = 18\tau_{d,\text{switch}}/(7R)$ becomes the upper boundary for Case 5(b).

In summary, in Case 5, i.e., for $9\tau_{d,\text{switch}}/(5R) < F_X^c < 18\tau_{d,\text{switch}}/(7R)$, there are two global minima located at $\pm M_{Z,2}^c$ and one local minimum at 0. The shape of the normalized cost function is shown in Fig. 9(5).

Case 6: For $F_X^c = 18\tau_{d,\text{switch}}/(7R)$ all the minima calculated in Case 5(b) become global minima (Fig. 9(6)), i.e., $M_Z^{c*} = 0$ and $M_Z^{c*} = \pm M_{Z,2}^c = \pm F_X^c w/3$.

Case 7: This case is for $F_X^c > 18\tau_{d,\text{switch}}/(7R)$, in which a global minimum is located at $M_Z^{c*} = 0$ as shown in Fig. 9(7).

B. Remarks

Table II summarizes the feedforward F_X^c-based TV control strategy (called DT in the remainder) minimizing the drivetrain power losses, according to the results of Section IV-A. In Table II the absolute value is applied to F_X^c for extending the solutions to the case of regeneration. Note that in general $\tau_{d,\text{switch},t} \neq \tau_{d,\text{switch},g}$. Table II shows the existence of multiple M_Z^{c*} for a given F_X^c, and also a plurality of optimal wheel torque distributions generating the same M_Z^{c*}. In particular:

- Either the inner side or the outer side of the EV can be indifferently selected to produce M_Z^{c*} in the cases indicated as SS (single side), i.e., in which only one side of the EV is applying a traction or regenerative torque, while the drivetrains located on the other side are inactive.
- In the SWS cases either the front drivetrain or the rear drivetrain can be indifferently used within a side.
- The minimization of $\bar{J}$ implies the progressive switching of an increasing number of electric drivetrains with $|F_X^c|$

TABLE II
TV CONTROL STRATEGY FOR DRIVETRAIN POWER LOSS MINIMIZATION (DT)

Case	Overall traction force	Optimal yaw moment	Optimal allocation strategy	Optimal no. of wheels in traction or regeneration
1	$0 < |F_X^c| < \frac{\tau_{d,swtch}}{R}$	$M_Z^{c*} = \pm|F_X^c|w$	SS: SWS	1
2	$|F_X^c| = \frac{\tau_{d,\text{switch}}}{R}$	$-|F_X^c|w \le M_Z^{c*} \le |F_X^c|w$	BS: SWS+SWS or SS: SWS	1 or 2
3	$\frac{\tau_{d,\text{switch}}}{R} < |F_X^c| < \frac{9}{5}\frac{\tau_{d,\text{switch}}}{R}$	$M_Z^{c*} = \{0, \pm|F_X^c|w\}$	BS: SWS+SWS or SS: EDS	2
4	$|F_X^c| = \frac{9}{5}\frac{\tau_{d,\text{switch}}}{R}$	$M_Z^{c*} = \{0, \pm\frac{|F_X^c|w}{3}, \pm|F_X^c|w\}$	BS: SWS+SWS or BS: SWS+EDS or SS: EDS	2 or 3
5	$\frac{9}{5}\frac{\tau_{d,\text{switch}}}{R} < |F_X^c| < \frac{18}{7}\frac{\tau_{d,\text{switch}}}{R}$	$M_Z^{c*} = \pm\frac{|F_X^c|w}{3}$	BS: SWS+EDS	3
6	$|F_X^c| = \frac{18}{7}\frac{\tau_{d,\text{switch}}}{R}$	$M_Z^{c*} = \{0, \pm\frac{|F_X^c|w}{3}\}$	BS: EDS+EDS or BS: SWS+EDS	3 or 4
7	$|F_X^c| > \frac{18}{7}\frac{\tau_{d,\text{switch}}}{R}$	$M_Z^{c*} = 0$	BS: EDS+EDS	4

SS: torque demand applied to a single side; BS: torque demand applied to both sides; SWS: single wheel strategy within the considered side; EDS: even distribution strategy within the considered side.

(see the left column of Table II), independently of their location within the EV.

The plurality of M_Z^{c*} and optimal wheel torque distributions would disappear if the longitudinal and lateral tire slip power losses were included in $\bar{J}$. This observation is confirmed by the experimental results of Figs. 5 and 6, which show the existence of a single M_Z^{c*} for each a_Y. Based on this observation, an updated TV control algorithm is developed in the next section.

V. THE EFFECT OF TIRE SLIP

The following Sections V-A and V-B highlight the effect of the longitudinal and lateral tire slip power losses. To this purpose a quasi-static EV model is adopted, which is a simplified version of the one in [15]. The main benefit of such modeling approach is that it does not need the forward time integration of the equations of motion, and therefore can be easily coupled to optimization routines. The model includes the third order polynomial approximation of the electric drivetrain power loss characteristics (see (1)) of the EV demonstrator. A tire model linearized at the vertical tire loads for the relevant values of a_X and a_Y describes tire behavior in terms of longitudinal slip stiffness and cornering stiffness. The quasi-static model is used for the minimization of different combinations of power loss contributions, according to the methodology in [15], to get an insight into their effect on the optimal wheel torque distribution and yaw moment.

The analyses are used in Section V-C to synthesize a rule-based sub-optimal yaw moment controller, which, in addition to the drivetrain power losses, partially accounts for tire slip power losses.

A. Longitudinal Tire Slip

The longitudinal tire slip power loss of the i–th corner, $P_{\text{loss},LoS,i}$, is given by:

$$P_{\text{loss},LoS,i} = F_{X,i} v_{slip,X,i} \tag{40}$$

where $F_{X,i}$ is the longitudinal tire force, and $v_{slip,X,i}$ is the longitudinal slip speed. By considering a linearization of $F_{X,i}$ based on the longitudinal slip stiffness, it is possible to verify that $P_{\text{loss},LoS,i}$ is proportional to the square of the slip ratio. As a consequence, longitudinal tire slip has an influence on the
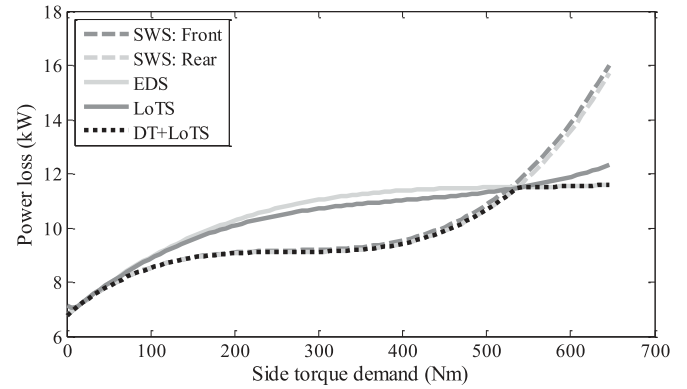

Fig. 10. Total power loss on a vehicle side as a function of $\tau_{d,l/r}$ for different wheel torque control allocation strategies at $V = 90$ km/h and $a_Y = 0$ m/s².

optimal torque shift, $\varepsilon_{d,l/r}^*$, within each side of the EV (see [20]). This is investigated in Fig. 10 with the quasi-static model at $V = 90$ km/h and $a_Y = 0$ m/s². The following wheel torque control allocation cases are compared: i) SWS: Front, in which the active drivetrain is the front one; ii) SWS: Rear, in which the active drivetrain is the rear one; iii) EDS; iv) LoTS, minimizing the longitudinal tire slip power losses; and v) DT+LoTS, minimizing the sum of the electric drivetrain power losses and longitudinal tire slip power losses. The DT case of Table II is implicitly included, as it implies the switching from SWS to EDS at $\tau_{d,\text{switch},t} = 536$ Nm.

The LoTS strategy tends to generate front-to-rear wheel torque distributions that are close to the front-to-rear vertical load distribution, to account for the variation of longitudinal slip stiffness with the vertical load transfer caused by a_X. However, as tire slip power losses are usually less significant than drivetrain power losses in most driving conditions, the power losses of LoTS are higher than those of DT and DT+LoTS for nearly the whole range of $\tau_{d,l/r}$ (the only exception is the region around $\tau_{d,\text{switch},t}$). Fig. 11 covers the range of $\tau_{d,l/r}$ in which the difference among DT and DT+LoTS is higher. Nevertheless, it shows that the DT+LoTS strategy produces a negligible reduction of the total power loss with respect to DT. In the context of an industrial implementation of the controller, these results do not justify the additional complexity
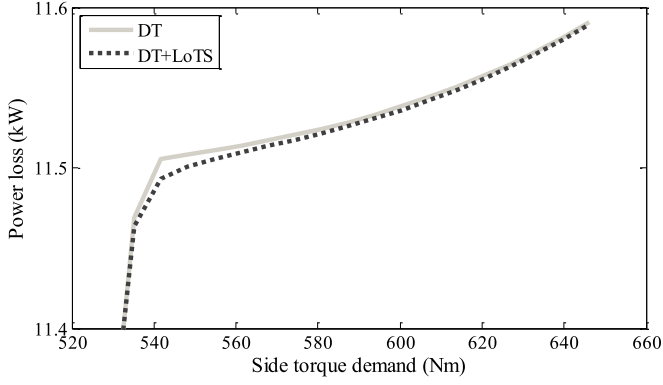
Fig. 11. Total power loss on a vehicle side as a function of $\tau_{d,l/r}$ for DT and DT+LoTS at $V = 90$ km/h and $a_Y = 0$ m/s^2.

of the direct minimization of the longitudinal slip power losses.

Fig. 10 also shows that SWS: Rear provides a marginal power loss reduction below $\tau_{d,\text{switch},t}$, with respect to SWS: Front. In fact, the same traction torque generates higher tire slip ratios – and thus power losses – on the axle with the smaller vertical tire load F_Z, i.e., the front one in the case study EV, because of its lower longitudinal slip stiffness. Based on this, the important conclusion is that in the DT strategy of Table II the SWS cases can be efficiently dealt with by activating the drivetrain of the corner with the greater F_Z (assuming equal tires on the front and rear axles).

B. Lateral Tire Slip

The lateral tire slip power loss of the i–th corner, $P_{\text{loss},LaS,i}$, is given by:

$$P_{\text{loss},LaS,i} = F_{Y,i} v_{slip,Y,i} \tag{41}$$

where $F_{Y,i}$ is the lateral tire force, and $v_{slip,Y,i}$ is the lateral slip speed. By considering a linearization of $F_{Y,i}$ based on the cornering stiffness, it is possible to verify that $P_{\text{loss},LaS,i}$ is proportional to the square of the slip angle. Fig. 12(a) plots the lateral tire slip power loss as a function of M_Z^c, calculated with the quasi-static model at $V = 60$ km/h, $a_X = 0.5$ m/s^2 and $a_Y = 4$ m/s^2. The control yaw moment minimizing the lateral tire slip power losses, $M_{Z,\alpha}^{c*}$, implies a neutral cornering behavior of the EV, i.e., a condition of equal slip angles on the front and rear tires. This is consistent with the simulation results in [30]. Since the understeer gradient of the BV depends on a_X and a_Y (e.g., see Fig. 4), $M_{Z,\alpha}^{c*}$ changes with the operating condition of the EV.

Interestingly, the theory discussed in Section IV and the trends in Fig. 12(a) and (b) explain the experimental results in Figs. 5 and 6, with the presence of a local minimum and an absolute minimum approximately located at the same absolute value of the reference yaw moment. In fact, the location of the absolute value of the optimal yaw moment is mainly determined by the drivetrain power losses, and is therefore symmetrical with respect to the condition of zero yaw moment. The tire slip power losses provoke the difference in the total power losses,
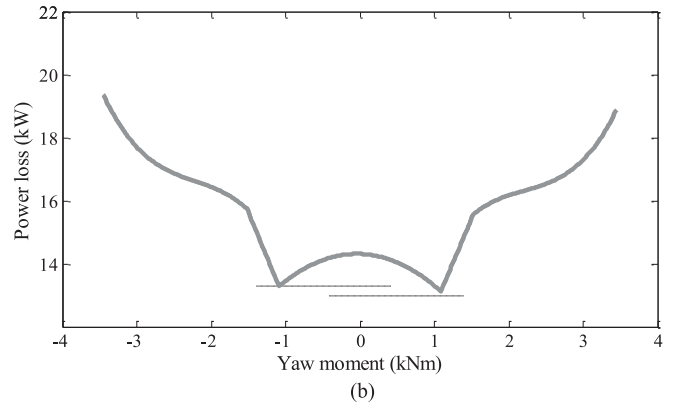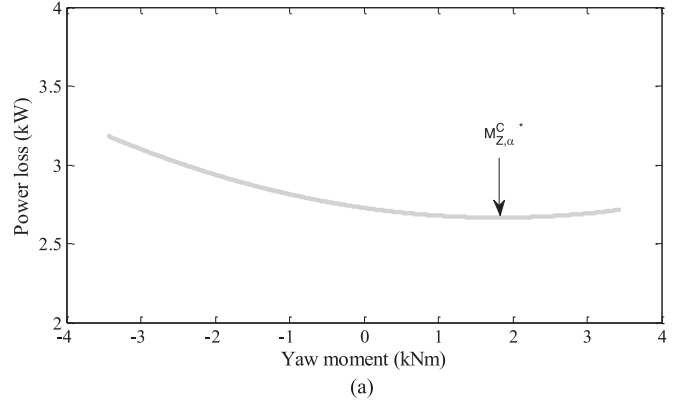

Fig. 12. (a) Tire slip power loss and (b) total power loss as a function of M_Z^c at $V = 60$ km/h, $a_X = 0.5$ m/s^2 and $a_Y = 4$ m/s^2. The drivetrain power loss characteristics are considered to be equal for traction and regeneration.

and thus power consumption, between the two minima, which was pointed out in the discussion of the experimental results on the vehicle demonstrator. The important conclusion is that in the DT strategy of Table II the cases with multiple M_Z^{c*} can be dealt with by selecting the value of M_Z^{c*} that is closest to $M_{Z,\alpha}^{c*}$.

C. The Sub-Optimal Energy-Efficient TV Controller

Table III reports the rule-based sub-optimal TV control strategy for the case study EV, minimizing the drivetrain power losses and selecting the best solution in terms of tire slip power losses among the redundant cases of Table II. In particular, the four columns of Table III report: i) the numbering of the cases of the rule-based sub-optimal TV control strategy; ii) the intervals of total longitudinal force, $|F_X^c|$, associated with the different cases. These intervals are functions of the switching torque, $\tau_{d,\text{switch}}$; iii) the corresponding formulation of the reference yaw moment of the TV system, M_Z^{c*}; and iv) the indication of the corresponding wheel torque allocation strategy, i.e., which drivetrains are used to generate M_Z^{c*}.

The result is sub-optimal with respect to the minimization of the total power loss, but provides a simple analytical solution that is effective if the drivetrain power losses are greater than the tire slip power losses, which is true for most conditions. This is achieved by: i) choosing the value of M_Z^{c*} that is closest to $M_{Z,\alpha}^{c*}$ within each range of F_X^c. For the specific case study EV, which is understeering, this means selecting the most destabilizing M_Z^{c*}

| Case	Overall traction force	Sub-optimal yaw moment	Sub-optimal allocation strategy
1	$0 < |F_X^c| \leq \dfrac{\tau_{d,\text{switch}}}{R}$	$M_Z^{c*} = |F_X^c|w$ if $a_Y > 0$ $M_Z^{c*} = -|F_X^c|w$ if $a_Y < 0$	Outer front wheel if $F_{Z,R} \leq F_{Z,F}$ Outer rear wheel if $F_{Z,R} > F_{Z,F}$
2	$\dfrac{\tau_{d,\text{switch}}}{R} < |F_X^c|$ $\leq \dfrac{9}{5}\dfrac{\tau_{d,\text{switch}}}{R}$	$M_Z^{c*} = |F_X^c|w$ if $a_Y > 0$ $M_Z^{c*} = -|F_X^c|w$ if $a_Y < 0$	Outer EV side with EDS
3	$\dfrac{9}{5}\dfrac{\tau_{d,\text{switch}}}{R} < |F_X^c|$ $\leq \dfrac{18}{7}\dfrac{\tau_{d,\text{switch}}}{R}$	$M_Z^{c*} = \dfrac{|F_X^c|w}{3}$ if $a_Y > 0$ $M_Z^{c*} = -\dfrac{|F_X^c|w}{3}$ if $a_Y < 0$	Outer EV side with EDS + Inner front wheel if $F_{Z,R} \leq F_{Z,F}$ Inner rear wheel if $F_{Z,R} > F_{Z,F}$
4	$|F_X^c| > \dfrac{18}{7}\dfrac{\tau_{d,\text{switch}}}{R}$	$M_Z^{c*} = 0$	BS with EDS
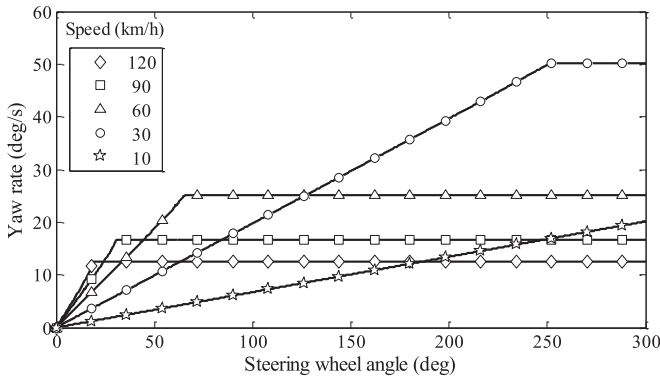
Fig. 13.   Example of set of r_{ref} characteristics corresponding to the sub-optimal solution.

between those in Table II; and ii) selecting the optimal wheel within each side of the EV for the SWS cases, i.e., by applying the whole drivetrain torque on the wheel with the greater vertical load within that side. In Table III $F_{Z,F}$ and $F_{Z,R}$ indicate the vertical load on the front and rear tires on the specific side. These can be easily estimated online from a_X, a_Y, and V. This approach allows:

- The synthesis of an energy-efficient feedforward M_Z^{c*}, which depends only on F_X^c, i.e., on the position of the accelerator and brake pedals and the EV drivability map. M_Z^{c*} can be directly implemented within Layer 2 of Fig. 1.
- The derivation of an energy-efficient r_{ref} look-up table that can be included in an existing TV control architecture (see Layer 1 of Fig. 1) based on yaw rate feedback control, thus providing a new eco-friendly driving mode. The look-up table (e.g., see Fig. 13) is obtained by imposing the M_Z^{c*} values of Table III in the quasi-static model.
- The definition of an energy-efficient wheel torque control allocation strategy within each side of the EV, based on SWS or EDS depending on $|\tau_{d,l/r}|$ (see Layer 3 of Fig. 1).

The following remarks must be considered with respect to the algorithm in Table III:

- Without proper adaptations, the derived $M_Z^{c*}(F_X^c)$ characteristics would give origin to discontinuities and drivability issues on a real EV subject to the continuous variations of wheel torque demand typical of normal driving. For example, the practical implementation of the controller must include a progressive transition from the condition of zero yaw moment for straight line EV operation to the condition of destabilizing yaw moment in cornering. Smooth transitions in M_Z^c and r_{ref} must also be implemented between Case 2 ($M_Z^{c*} = |F_X^c|w$) and Case 3 ($M_Z^{c*} = |F_X^c|w/3$), and between Case 3 and Case 4 ($M_Z^{c*} = 0$).
- The TV controller can be used also with different power loss characteristics in traction and regeneration by calculating $\tau_{d,\text{switch},t} \neq \tau_{d,\text{switch},g}$.
- An EV with drivetrains with convex power loss characteristics at each speed meets the condition $\tau_{d,\text{switch}} = 0 \, \forall \, V$. Thus, the optimal solution corresponds to Case 4 in Table III. On the other hand, if the drivetrain power loss characteristics have a non-convex shape regardless of V (which is an unlikely case, based on the typical electric motor efficiency characteristics), the condition $\tau_{d,\text{switch}} = \infty \, \forall \, V$ is satisfied. As a consequence, the optimal solution is given by Case 1 in Table III.
- Specific analyses with non-linear vehicle models have been carried out to investigate the sensitivity of the proposed control algorithm in Table III with respect to the variation of the tire-road friction conditions. The results show that the optimal control yaw moment does not substantially change with the available friction level, since the drivetrain power losses remain the prevailing contribution for the specific vehicle, i.e., the variation of the tire slip power losses with the reference yaw moment is less significant than the variation of the drivetrain power losses. Future work will focus on the possibility of extending the performance of the proposed energy-efficient algorithm applied to the electric vehicle operation in off-road conditions.
- The other sources of vehicle power loss do not have any effect on the optimal yaw moment and control allocation algorithm. For example, this applies to the power losses associated with the aerodynamics and battery pack, since they are increasing functions of vehicle speed or total drivetrain input power.

VI. PRELIMINARY EXPERIMENTAL ASSESSMENT

This section preliminarily assesses the performance of the sub-optimal TV strategy of Section V-C through experimental data from the EV demonstrator (Fig. 2). Fig. 14 plots the $F_X^c(a_Y)$ characteristic measured during a $\sim$60 m radius skid-pad test. F_X^c increases with a_Y, because of the increase of the aerodynamic drag force, rolling resistance torque and tire slip power losses. The figure also reports the three F_X^c thresholds, i.e., $\tau_{d,\text{switch},t}/R$, $9\tau_{d,\text{switch},t}/(5R)$ and $18\tau_{d,\text{switch},t}/(7R)$, determining the boundaries of Cases 1-4 in Table III. Such thresholds vary with a_Y because of the variation of $\tau_{d,\text{switch},t}$ with V.
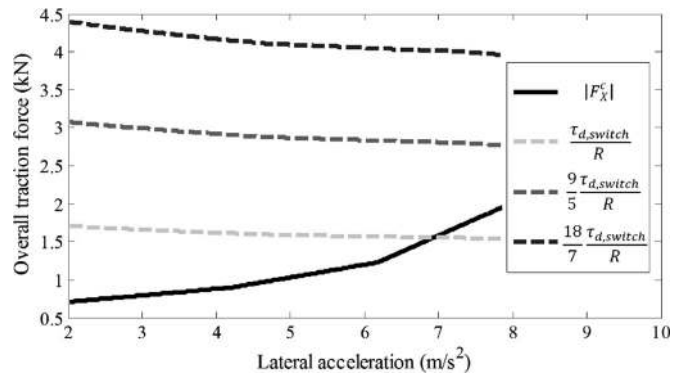
Fig. 14. Comparison between the thresholds in Table III and F_X^c during a ~60 m radius skid-pad test.
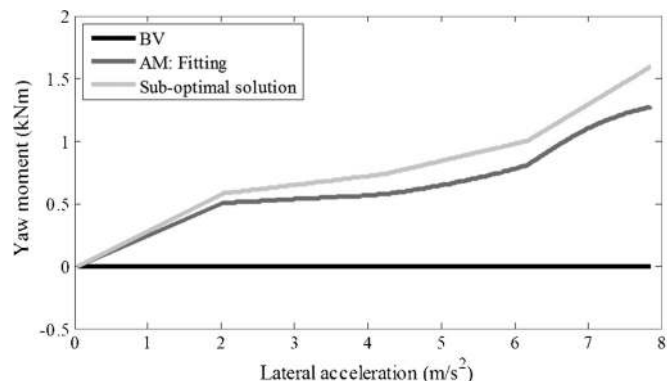

Fig. 15. Comparison between the BV, AM and sub-optimal solution in terms of yaw moment characteristic during a 60 m radius skid-pad test.
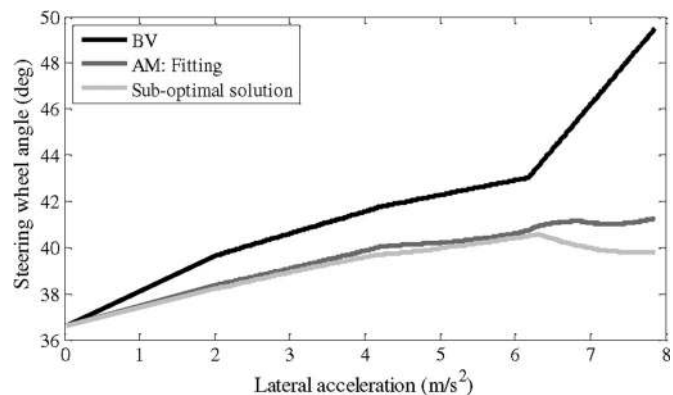

Fig. 16. Comparison between the BV, AM and sub-optimal solution in terms of understeer characteristic during a ~60 m radius skid-pad test.

TABLE IV
EXPERIMENTAL AVERAGE POWER CONSUMPTION DURING
A SKID-PAD LAP (~60 m RADIUS)

Lateral acceleration (m/s^2)	Power consumption (kW)		Degradation of SOS wrt AM (%)
	AM	SOS	
2	7.52	7.59	0.93
4	15.05	15.28	1.53
6	26.09	26.68	2.26
8	45.51	45.66	0.33

providing the minimum energy consumption; and iii) the TV controlled EV using the sub-optimal algorithm in Table III. The characteristics of ii) and iii) are very close to each other. In particular, they are substantially coincident for $a_Y < 6.2$ m/s², which corresponds to more than 2/3 of the achievable a_Y range in high tire-road friction conditions. Overall, ii) and iii) bring a significant reduction of the energy consumption, which is clear from the iso-lines in Fig. 6. The marginal difference between the experimental AM and the analytical sub-optimal solution is mainly caused by the fact that the latter is aimed at the minimization of the drivetrain power losses, and considers the tire slip power losses solely for the arbitration among the multiple drivetrain-based optimal solutions.

To assess the efficiency implications of the understeer characteristic of the sub-optimal algorithm, i.e., without considering the effect of the wheel torque allocation, Table IV reports the comparison of the experimental average power consumption for the ~60 m skid pad tests of Section II-B for: i) the electric vehicle tracking the AM understeer characteristic; and ii) the same vehicle tracking the understeer characteristic of the sub-optimal solution of Table III, indicated as SOS, and using the EDS as control allocation strategy. Depending on the lateral acceleration level, the power input difference between the AM and SOS ranges between 0.33% and 2.26%, which is considerably less than the difference, ranging from 5.40% to 12.31% (see Table I), between the BV and AM. This is an important preliminary experimental confirmation of the validity of the proposed explicit solution.

The sub-optimal TV control strategy was preliminarily assessed in terms of wheel torque control allocation as well. For example, at $a_Y = 2$ m/s² the adoption of SWS on the outer side, with the deactivation of all the other EV drivetrains, according to Case 1 of Table III, implies an energy consumption of 69.1 Wh along one ~60 m skid-pad lap with $M_Z^{c*} \cong 450$ Nm. This represents a further 3.1% saving with respect to the AM case of Table I, obtained with EDS, and a total saving of 8.5% with respect to the BV.

VII. CONCLUSIONS

This study allows the following conclusions:
- The experimental results on a torque-vectoring controlled electric vehicle with four identical drivetrains show that the power consumption is minimized for a specific desta-

The significant increase of F_X^c during the test (approximately by a factor 3) prescribes the transition from Case 1 to Case 2 of Table III at $a_Y \cong 7$ m/s². In Case 1, F_X^c is entirely generated by the rear outer wheel, while in Case 2, F_X^c is generated by the two outer wheels with EDS. In both cases, the yaw moment is destabilizing.

Figs. 15 and 16 report $M_Z^c(a_Y)$ and $\delta(a_Y)$ for: i) the BV; ii) the TV controlled EV with the reference understeer characteristic corresponding to the AM case of Section II-B, i.e., the EV with the experimentally derived $M_Z^c(a_Y)$ characteristic

bilizing yaw moment, which is a function of the operating condition of the vehicle. The power consumption characteristics also exhibit a local minimum for a stabilizing yaw moment, which has approximately the same absolute value as the optimal destabilizing yaw moment at that lateral acceleration.

- A torque-vectoring control algorithm minimizing the total electric drivetrain power loss was mathematically derived. The analysis demonstrated the existence of multiple equivalent solutions. These imply the progressive activation of an increasing number of drivetrains, with the increase of the absolute value of the total longitudinal force demand.
- Tire slip power losses can be used for the selection of the best solution among the multiple solutions of the algorithm minimizing the electric drivetrain power losses. This leads to the formulation of a rule-based sub-optimal torque-vectoring control strategy aimed at reducing the total power consumption.
- The effectiveness of the sub-optimal control strategy was experimentally validated in steady-state cornering conditions, leading to energy savings >8% with respect to the baseline vehicle.

Further research will focus on: i) the more extensive experimental validation of the proposed sub-optimal torque-vectoring controller; ii) the detailed analysis of the required adaptations for achieving good drivability characteristics for the whole range of operating conditions; and iii) the assessment and adaptation of the sub-optimal controller to operating conditions with significant tire slip power losses.

APPENDIX

A. Power Loss Characteristic on a Vehicle Side

The power loss on a side (e.g., the left-hand side) is a monotonically increasing function of the torque demand in the case of equal drivetrains, i.e., if $a_{1,t/g} = a_{3,t/g}$, $b_{1,t/g} = b_{3,t/g}$ and $c_{1,t/g} = c_{3,t/g}$ (d_1 can differ from d_3 because of the effect of vertical tire load on rolling resistance). Thus it is:

$$A = \frac{3}{4}a_{1,t/g}\tau_{d,l}^2 + 3a_{1,t/g}\varepsilon_{d,l}^2 + b_{1,t/g}|\tau_{d,l}| + c_{1,t/g}$$

$$B = \left(6a_{1,t/g}|\tau_{d,l}| + 4b_{1,t/g}\right)|\varepsilon_{d,l}| \tag{42}$$

If $|\tau_{d,l}| < \tau_{d,\text{switch},t/g}$:

$$\frac{\partial P_{\text{loss},l,t/g}}{\partial|\tau_{d,l}|} = A + \frac{\partial|\varepsilon_{d,l}|}{\partial|\tau_{d,l}|}B = 3a_{1,t/g}\tau_{d,l}^2 + 2b_{1,t/g}|\tau_{d,l}|$$

$$+ c_{1,t/g} > 0 \tag{43}$$

If $|\tau_{d,l}| \geq \tau_{d,\text{switch},t/g}$:

$$\frac{\partial P_{\text{loss},l,t/g}}{\partial|\tau_{d,l}|} = A = \frac{3}{4}a_{1,t/g}\tau_{d,l}^2 + b_{1,t/g}|\tau_{d,l}| + c_{1,t/g} > 0 \tag{44}$$

(43) and (44) are satisfied because of the condition $b_{1,t/g}^2 < 3a_{1,t/g}c_{1,t/g}$, which must be met to have $\partial P_{\text{loss},1,t/g}/\partial\tau_{d,1,t/g} > 0$.

B. Cost Function Calculations

Conditions for Case 3(b):

$$\bar{J}_{\text{SWS+SWS}}\left(0, F_X^c\right) = \frac{F_X^{c3}R^3a_1 + 2F_X^{c2}R^2b_1 + 4F_X^c Rc_1}{4} \tag{45}$$

$$\bar{J}_{\text{SWS+EDS}}\left(M_{Z,2}^c, F_X^c\right) = \frac{F_X^{c3}R^3a_1 + 3F_X^{c2}R^2b_1 + 9F_X^c Rc_1}{9} \tag{46}$$

$$\bar{J}_{\text{SWS+SWS}}\left(0, F_X^c\right) < \bar{J}_{\text{SWS+EDS}}\left(M_{Z,2}^c, F_X^c\right)$$

$$\Leftrightarrow -5F_X^{c3}R^3a_1 - 6F_X^{c2}R^2b_1 > 0 \rightarrow F_X^c < \frac{9}{5}\frac{\tau_{d,\text{switch}}}{R} \tag{47}$$

Conditions for Case 5(a):

$$\bar{J}_{\text{EDS+EDS}}\left(0, F_X^c\right) = \frac{a_1 F_X^{c3}R^3 + 4b_1 F_X^{c2}R^2 + 16c_1 F_X^c R}{16} \tag{48}$$

$$\bar{J}_{\text{SWS+ESD}}\left(M_{Z,2}^c, F_X^c\right) < \bar{J}_{\text{EDS+EDS}}\left(0, F_X^c\right)$$

$$\Leftrightarrow 7F_X^c Ra_1 + 12b_1 < 0 \rightarrow F_X^c < \frac{18}{7}\frac{\tau_{d,\text{switch}}}{R} \tag{49}$$

REFERENCES

[1] Y. Wang, B. M. Nguyen, H. Fujimoto, and Y. Hori, "Multirate estimation and control of body sideslip angle for electric vehicles based on onboard vision system," *IEEE Trans. Ind. Electron.*, vol. 61, no. 2, pp. 1133–1143, Feb. 2014.

[2] B. Lenzo, A. Sorniotti, P. Gruber, and K. Sannen, "On the experimental analysis of single input single output control of yaw rate and sideslip angle," *Int. J. Automotive Technol.*, vol. 18, no. 5, pp. 799–811, 2017.

[3] A. Wong, D. Kasinathan, A. Khajepour, S. K. Chen, and B. Litkouhi, "Integrated torque vectoring and power management framework for electric vehicles," *Control Eng. Practice*, vol. 48, pp. 22–36, 2016.

[4] R. de Castro, "Minimum-time manoeuvring in electric vehicles with four wheel-individual-motors," *Veh. Syst. Dyn.*, vol. 52, no. 6, pp. 824–846, 2014.

[5] E. N. Smith, D. Tavernini, E. Velenis, and D. Cao, "Evaluation of optimal yaw rate reference for closed-loop electric vehicle torque vectoring," in *Proc. 13th Int. Symp. Adv. Veh. Control*, 2016, pp. 619–624.

[6] V. Ivanov, D. Savitski, and B. Shyrokau, "A survey of traction control and antilock braking systems of full electric vehicles with individually controlled electric motors," *IEEE Trans. Veh. Technol.*, vol. 64, no. 9, pp. 3878–3896, Sep. 2015.

[7] L. De Novellis, A. Sorniotti, and P. Gruber, "Driving modes for designing the cornering response of fully electric vehicles with multiple motors," *Mech. Syst. Signal Process.*, vol. 64-65, pp. 1–15, 2015.

[8] L. De Novellis *et al.*, "Direct yaw moment control actuated through electric drivetrains and friction brakes: Theoretical design and experimental assessment," *Mechatronics*, vol. 26, pp. 1–15, 2015.

[9] L. De Novellis, A. Sorniotti, P. Gruber, and A. Pennycott, "Comparison of feedback control techniques for torque-vectoring control of fully electric vehicles," *IEEE Trans. Veh. Technol.*, vol. 63, no. 8, pp. 3612–3623, Oct. 2014.

[10] Q. Lu, P. Gentile, A. Tota, A. Sorniotti, P. Gruber, F. Costamagna, and J. De Smet, "Enhancing vehicle cornering limit through sideslip and yaw rate control," *Mech. Syst. Signal Process.*, vol. 75, pp. 455–472, 2016.

[11] Q. Lu, A. Sorniotti, P. Gruber, J. Theunissen, and J. De Smet, "H∞ loop shaping for the torque-vectoring control of electric vehicles: Theoretical design and experimental assessment," *Mechatronics*, vol. 35, pp. 32–43, 2016.

[12] T. A. Johansen and T. I. Fossen, "Control allocation—A survey," *Automatica*, vol. 49, no. 5, pp. 1087–1103, 2013.

[13] Y. Suzuki, Y. Kano, and M. Abe, "A study on tyre force distribution controls for full drive-by-wire electric vehicle," *Veh. Syst. Dyn.*, vol. 52, no. 1, pp. 235–250, 2014.

[14] B. Li, A. Goodarzi, A. Khajepour, S. K. Chen, and B. Litkouhi, "An optimal torque distribution control strategy for four-independent wheel drive electric vehicles," *Veh. Syst. Dyn.*, vol. 53, no. 8, pp. 1–18, 2015.

[15] L. De Novellis, A. Sorniotti, and P. Gruber, "Wheel torque distribution criteria for electric vehicles with torque-vectoring differentials," *IEEE Trans. Veh. Technol.*, vol. 63, no. 4, pp. 1593–1602, May 2014.

[16] P. Tøndel and T. A. Johansen, "Control allocation for yaw stabilization in automotive vehicles using multiparametric nonlinear programming," in *Proc. Amer. Control Conf.*, 2005, pp. 453–458.

[17] J. Tjonnas and T. A. Johansen, "Stabilization of automotive vehicles using active steering and adaptive brake control allocation," *IEEE Trans. Control Syst. Technol.*, vol. 18, no. 3, pp. 545–558, May 2010.

[18] R. Wang, Y. Chen, D. Feng, X. Huang, and J. Wang, "Development and performance characterization of an electric ground vehicle with independently actuated in-wheel motors," *J. Power Sources*, vol. 196, pp. 3962–3971, 2011.

[19] Y. Chen and J. Wang, "Adaptive energy-efficient control allocation for planar motion control of over-actuated electric ground vehicles," *IEEE Trans. Control Syst. Technol.*, vol. 22, no. 4, pp. 1362–1373, Jul. 2014.

[20] A. Pennycott, L. De Novellis, P. Gruber, and A. Sorniotti, "Sources of energy loss during torque-vectoring for fully electric vehicles," *Int. J. Veh. Des.*, vol. 67, no. 2, pp. 157–177, 2014.

[21] A. Pennycott, L. De Novellis, A. Sabbatini, P. Gruber, and A. Sorniotti, "Reducing the motor power losses of a four-wheel drive, fully electric vehicle via wheel torque allocation," *Proc. Inst. Mech. Eng., Part D, J. Automobile Eng.*, vol. 228, no. 7, pp. 830–839, 2014.

[22] X. Yuan and J. Wang, "Torque distribution strategy for a front- and rear-wheel-driven electric vehicle," *IEEE Trans. Veh. Technol.*, vol. 61, no. 8, pp. 3365–3374, Oct. 2012.

[23] H. Fujimoto and S. Harada, "Model-based range extension control system for electric vehicles with front and rear driving-braking force distributions," *IEEE Trans. Ind. Electron.*, vol. 62, no. 5, pp. 3245–3254, May 2015.

[24] Y. Chen and J. Wang, "Design and experimental evaluations on energy efficient control allocation methods for overactuated electric vehicles: Longitudinal motion case," *IEEE/ASME Trans. Mechatron.*, vol. 19, no. 2, pp. 538–548, Apr. 2014.

[25] Y. Chen and J. Wang, "Fast and global optimal energy-efficient control allocation with applications to over-actuated electric ground vehicles," *IEEE Trans. Control Syst. Technol.*, vol. 20, no. 5, pp. 1202–1211, Sep. 2012.

[26] A. M. Dizqah, B. Lenzo, A. Sorniotti, P. Gruber, S. Fallah, and J. De Smet, "A fast and parametric torque distribution strategy for four-wheel-drive energy-efficient electric vehicles," *IEEE Trans. Ind. Electron.*, vol. 63, no. 7, pp. 4367–4376, Jul. 2016.

[27] G. De Filippis, B. Lenzo, A. Sorniotti, P. Gruber, K. Sannen, and J. De Smet, "On the energy efficiency of electric vehicles with multiple motors," in *Proc. IEEE Veh. Power Propulsion Conf.*, 2016, pp. 1–6.

[28] T. Kobayashi and E. Katsuyama, "Direct yaw moment control and power consumption of in-wheel motor vehicle in steady-state turning," *Veh. Syst. Dyn.*, vol. 55, pp. 104–120, 2017.

[29] T. Kobayashi, E. Katsuyama, H. Sugiura, E. Ono, and M. Yamamoto, "Study on direct yaw moment and power consumption of an in-wheel motor vehicle," *R&D Rev. Toyota CRDL*, vol. 47, no. 3, pp. 51–59, 2016.

[30] T. Kobayashi, H. Suguira, E. Ono, E. Katsuyama, and M. Yamamoto, "Efficient direct yaw moment control of in-wheel motor vehicle," in *Proc. 13th Int. Symp. Adv. Veh. Control*, 2016, pp. 631–636.

[31] B. Lenzo *et al.*, "Torque distribution strategies for energy-efficient electric vehicles with multiple drivetrains," *ASME J. Dyn. Syst., Meas. Control*, vol. 139, no. 12, pp. 121004–121004-13, 2017.

[32] T. Goggia *et al.*, "Integral sliding mode for the torque-vectoring control of fully electric vehicles: Theoretical design and experimental assessment," *IEEE Trans. Vehicular Technol.*, vol. 64, no. 5, pp. 1701–1715, May 2015.

[33] G. Genta, *Motor Vehicle Dynamics: Modeling and Simulation*, Singapore: World Sci., 1997.

[34] W. F. Milliken and D. L. Milliken, *Race Car Vehicle Dynamics*, Troy, MI, USA: SAE Int., 1995.

Giovanni De Filippis received the M.Sc. degree in mechanical engineering and the Ph.D. degree in mechanical and management engineering from the Politecnico di Bari, Bari, Italy, in 2011 and 2015, respectively. In 2015, he was a Research Fellow in advanced vehicle engineering with the University of Surrey, Guildford, U.K. He is currently with McLaren Automotive Ltd., Woking, U.K. His main research interests include vehicle dynamics control and system identification.

Basilio Lenzo (M'13) received the M.Sc. degree in mechanical engineering from the University of Pisa and Scuola Superiore Sant'Anna, Pisa, Italy, in 2010, and the Ph.D. degree in robotics from Scuola Superiore Sant'Anna, Pisa, Italy, in 2013. In 2015, he was a Research Fellow in advanced vehicle engineering with the University of Surrey, Guildford, U.K. He is currently a Senior Lecturer with Sheffield Hallam University, Sheffield, U.K. His current research interests include vehicle dynamics, simulation and control.

Aldo Sorniotti (M'12) received the M.Sc. degree in mechanical engineering and the Ph.D. degree in applied mechanics from the Politecnico di Torino, Turin, Italy, in 2001 and 2005, respectively. He is currently a Professor in advanced vehicle engineering with the University of Surrey, Guildford, U.K., where he leads the Centre for Automotive Engineering. His research interests include vehicle dynamics control and transmission systems for electric and hybrid electric vehicles.

Patrick Gruber received the M.Sc. degree in motorsport engineering and management from Cranfield University, Cranfield, U.K., in 2005, and the Ph.D. degree in mechanical engineering from the University of Surrey, Guildford, U.K., in 2009. He is currently a Senior Lecturer in advanced vehicle systems engineering with the University of Surrey. His current research interests include tire dynamics and development of novel tire models.

Wouter De Nijs received the M.Sc. degree in mechanical engineering in the field of mechatronics from the KU Leuven, Leuven, Belgium, in 2006. He is a Core Lab Manager with Flanders Make, the Flemish Strategic Research Centre for the Manufacturing Industry, Leuven, Belgium, where his lab performs pre-competitive industry driven research on novel sensing, monitoring, control and decision making solutions in the application fields of vehicles-, machines- and factories-of-the-future.